Elements of Gamma Camera and SPECT Systems

10

Magdy M. Khalil

Contents

M.M. Khalil
Biological Imaging Centre, MRC/CSC, Imperial College London, Hammersmith Campus, Du Cane Road, W12 0NN London, UK
e-mail: magdy.khalil@imperial.ac.uk

10.1 Introduction

Nuclear medicine provides noninvasive imaging tools to detect a variety of human diseases. The two major components of these imaging procedures are radiopharmaceuticals and an imaging system. The latter is a position-sensitive detector that relies on detecting gamma photons emitted from the administered radionuclide. Many single-photon and positron emitters are used in the nuclear medicine clinic. The radiopharmaceuticals are designed for tracing many pathophysiologic as well as molecular disorders and utilize the penetrating capability of gamma rays to functionally map the distribution of the administered compound within different biological tissues. The imaging systems used for detection of radionuclide-labeled compounds are special devices called scintillation cameras or positron emission tomographic (PET) scanners. These devices have passed through a number of developments since their introduction in the late 1960s and have had a significant impact on the practice and diagnostic quality of nuclear medicine.

The birth of nuclear medicine instrumentation dates to 1925; Blumgert and his coworker Otto C. Yens had modified the cloud chamber to measure the circulation time using an arm-to-arm method [1]. They used a mixture of radium decay products that emit beta and gamma rays. Blumgert postulated some assumptions for designing a detector or measurement technique that still hold true when compared with requirements of today: The technique must be objective and noninvasive and have the capability to measure the arrival of the substance automatically [1]. In 1951, Benedict Cassen introduced the rectilinear scanner to register a distribution of radioactivity accumulated in a human body. To scan a given area of interest, the scanner moves along a straight line collecting activity point by point. The scanner then moves over a predetermined distance and moves back in the opposite direction to span an equivalent length. This process is continued until the device scans the desired area of interest. Images are formed by a mechanical relay printer that prints the acquired events in a dot style. Initially, the scanner was used to scan iodine-131 in thyroid patients [2]. A major drawback of the

rectilinear scanner was the long acquisition time since radiation events are registered point by point in a sequential manner, taking 60–90 min to determine the outline of the thyroid gland [2]. Low contrast and spatial resolution of the formed images were also disadvantages of the rectilinear scanner.

In 1953, Hal Anger (at the Donner Laboratory of the Lawrence Berkeley Laboratory, USA) developed the first camera in which a photographic x-ray film was in contact with an NaI(Tl) intensifying screen. He used a pinhole collimation and small detector size to project the distribution of gamma rays onto the scintillation screen [3]. Initially, the camera was used to scan patients administered therapeutic doses of ^{131}I. A disadvantage of this prototype was the small field of view of the imaging system (4-in. diameter). Moreover, good image quality was difficult to obtain unless high doses were administered along with long exposure times. In 1958, Anger succeeded in developing the first efficient scintillation camera, which was then called by his name, the Anger camera. Marked progress in detection efficiency was realized as he used an NaI(Tl) crystal, photomultiplier tubes (PMTs), and a larger field of view.

Recent years have witnessed remarkable advances in the design of the gamma camera and single-photon emission computed tomographic (SPECT) systems. These were not only concerned with clinical scanners but also small-animal SPECT systems, providing a new era of molecular and imaging innovations using compounds labeled with single-photon emitters. Unlike PET, SPECT compounds in theory can provide images with high spatial resolution and the ability to follow the tracer uptake over more time intervals, including hours and days. PET imaging lacks such a property due to the short half-lives of most tracers. In contrast to PET scanners, dual tracer imaging capability can be easily achieved using SPECT compounds and a gamma camera system equipped with a multi-channel analyzer.

While most of the present and commercially available gamma cameras are based largely on the original design made by Anger using sodium iodide crystal, successful trials of new imaging systems that suit either specific imaging requirements or improved image quality and enhanced diagnostic accuracy are emerging. One of these changes is the trend toward manufacturing a semiconductor gamma camera with performance characteristics superior to those achieved by the conventional design. Organ-specific or dedicated designs are now well recognized in cardiac as well as scintimammography. Both imaging procedures were shown to be superior, with such systems realizing better imaging quality and enhancement of lesion detectability. When these approaches were implemented and introduced into the clinic, significant changes in data interpretation and diagnostic outcome were achieved.

For breast imaging, a miniaturized version of the gamma camera based either on semiconductor technology or scintillation detectors has been commercially available. Another example is the cardiac-specific gamma camera, and a growing number of dedicated cardiac systems have been under development (some of them are combined with computed tomography [CT]) to improve the detection task. The developments in this area are concerned not only with hardware components but also some successful approaches to improve diagnostic images using resolution recovery and subsequent reduction of imaging time or administered dose. It has become possible that some imaging systems can perform cardiac scanning in a significantly shorter scanning time than conventionally used. The utility of SPECT systems is increasing with the addition of anatomical imaging devices such as CT and magnetic resonance imaging (MRI), and this is covered in some detail in the last few sections of the chapter.

Now, there is also interest in using semiconductor photodetectors to replace the historical PMTs to provide compactness, portability, and reduction of space requirements along with features that allow incorporation in multimodality imaging devices. The next generation of SPECT and PET devices will exploit these characteristics to overcome the current performance limitations of both imaging modalities.

10.2 The Gamma Camera

10.2.1 Theory

The gamma camera is a medical radiation detection device of various hardware components such that each component has a specific role in the photon detection process. It is outside the scope of the chapter

to describe all these elements and their detailed functions. However, the principal components of the imaging system are described in addition to their relative contribution to image formation. Generally, these components are the collimator, crystal, PMT, preamplifier, amplifier, pulse height analyzer (PHA), position circuitry, computer system for data correction and image analysis, and ultimately a monitor for image display.

Briefly, once the patient has been injected and prepared for imaging, the first hardware component that is met by the incident photons is the collimator. The collimator determines the directionality of the incident photons and accordingly forms the hardware role in outlining the activity distribution within different organs. The accepted photons then interact with the detector crystal to produce scintillation light photons. The photomultiplier converts the light pulse into an electronic signal. Through a number of steps that involve an identification of the photon energy and event positioning, the scintillation site is determined, which in turn reflects the spatial position of the emitted photons.

The heart of the scintillation camera is a position-sensitive detector that can localize the interaction sites where incident photons imparted their energy. The conventional design of the gamma camera consists of a continuous structure of a scintillation crystal mapped by an array of PMTs. The last component is not a point or pencil-like photodetector, and size, shape, and the number of PMTs vary among manufacturers. Another point that should be mentioned is that the scintillation light emits a narrow beam of light photons; however, it diverges and spreads over the crystal and appears at the PMT end as a cone shape, illuminating more than one PMT. Most often, one PMT receives the maximum amount of light produced by the scintillation event; therefore, the site of interaction could be determined based on a single PMT signal [4]. The original design proposed by Anger is shown in Fig. 10.1.

To spatially determine a distribution of radioactivity inside a human organ, an electronic circuit that is able to localize the position of the emitted gamma radiations must exist in the detection system. The inclusion of all PMT signals should theoretically yield better precision in positioning measurements. However, as the distant PMTs receive little light, they contribute with less certainty to the identification process, leading to increased noise. This can be treated

by a thresholding process, by which the tube signals below a set value are either ignored or the tubes are adjusted by a threshold value [5, 6].

The output of the PMTs is mapped by a network of electric resistors. The resistors are weighted according to the spatial position of the PMTs in the x- and y-axes of the coordinate system of the array. This helps to identify the spatial position of an event based on the relative amount of current received by each resistor. The classical method of event positioning determination is the Anger logic centroid approach, by which each event results in four signals $X-$, $X+$, $Y-$, and $Y+$, and then applying a simple formula per coordinate to obtain the spatial position within the 2D (two-dimensional) matrix [1].

In the analog design of the gamma camera, three signals are detected. Two signals indicate the spatial position (X, Y), and one signal indicates the energy of the incident photon, Z-signal, or pulse height. The three signals are a mathematical analysis of the PMT output identified according to the positive and negative direction of the x ($x+$ and $x-$) and y ($y+$ and $y-$) coordinates. The energy is proportional to the amount of light produced in the crystal and with the energy deposited by the gamma radiation and computed by summing all the output signals of the involved PMTs. The position signal is divided by the energy signal so that the spatial coordinate signals become more independent of the energy signal. However, this simple process for event localization suffers from nonuniform spatial behavior, differences in PMT gain, and edge packing problems, which occurs when the scintillation event becomes close to the crystal edge. In the last situation, the positioning algorithm fails to accurately position the scintillation event as the light distribution from the scintillation site is asymmetric or truncated, leading to improper PMT position weighting and loss of spatial resolution. Furthermore, these problems associated with the detector peripheral regions cause loss of detection efficiency and a reduction of the imaging field of view. In gamma camera-based coincidence systems, this phenomenon could result in malfunctioning detector areas corrupting the reconstruction process.

In the digital gamma camera, the signal of the PMT is digitized by what is called an analog-to-digital converter (ADC). Further detector development has resulted in a process of digitizing the signal directly at the preamplifier output to couple each PMT to a
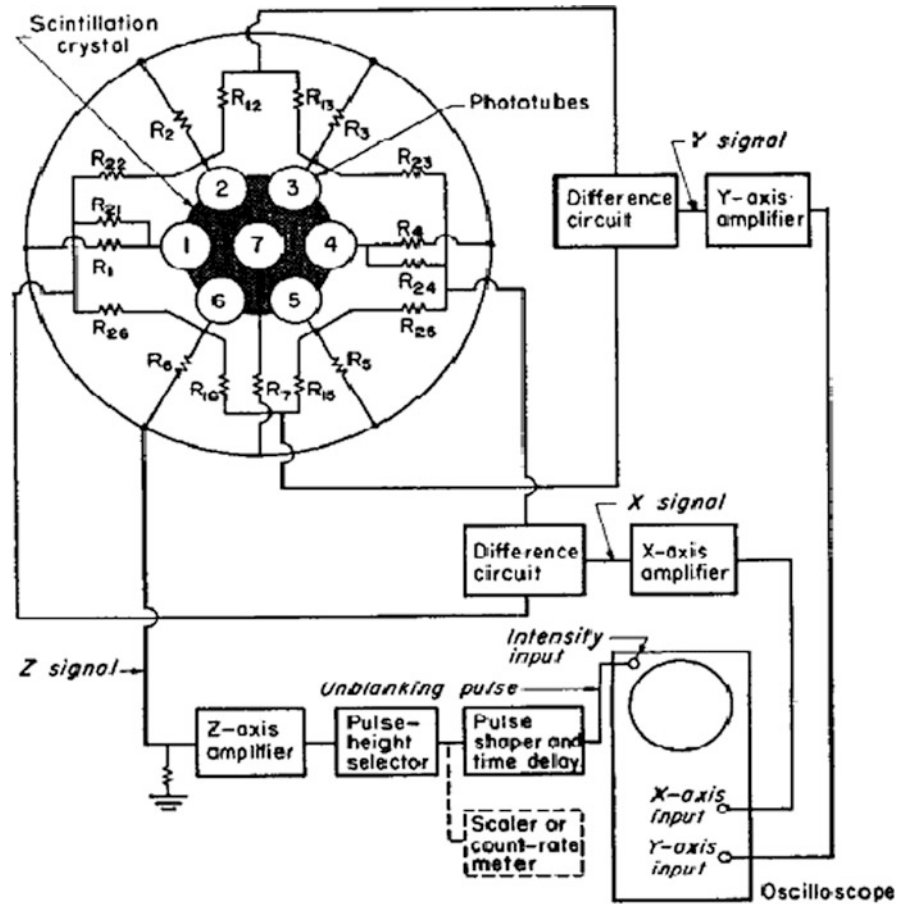
single ADC. In this situation, position information is no longer established using resistors and a summation circuit, but the localization circuitry has been totally replaced by a dedicated onboard computer [7].

After signal digitization, the determination of pulse position on the crystal is achieved using the "normalized position-weighted sum" circuit, in a fashion similar to the analog camera "Anger logic circuit," or by picking up a correction factor from lookup tables constructed previously in a calibration test. This process is implemented through a software program using mathematical algorithms. Other event-positioning methods were developed, such as detailed crystal mapping, Gaussian fitting, neural networks, maximum likelihood estimation, and distance-weighted algorithms applied in an iterative manner [5, 8]. The lookup correction tables contain information regarding the spatial distortion or camera nonlinearity for accurate determination of event position during routine patient acquisition. In the calibration process, the PMT response is calibrated to a spatial activity distributing with a well-defined pattern on the crystal surface [9].

10.2.2 Collimators

Gamma radiation emitted from a radioactive source are uniformly distributed over a spherical geometry. They are not like light waves, which can be focused into a certain point using optical lenses. Gamma radiation emitted from an administered radionuclide into a patient is detected by allowing those photons that pass through a certain direction to interact with the crystal. By this concept, we can collect and outline the radioactivity distributed within different tissues by a multihole aperture or what is called a collimator.

The collimator is an array of holes and septa designed with a specific geometric pattern on a slab of lead. The geometric design of the holes and septa determines the collimator type and function. Unfortunately, most gamma radiation emitted from an injected radionuclide cannot be detected by the gamma camera since many gamma rays do not travel in the directions provided by collimator holes. This is in great part due to the small solid angle provided by the collimator area in addition to the area occupied by the septal thickness. In the detection process for gamma rays, approximately 1 of every 100,000 photons is detected by the detector system, which is relatively inefficient process for gamma ray detection, leading to poor count statistics [10]. The collimator material is often made of lead due to its attenuation and absorption properties. Lead has a high atomic number ($Z = 82$) and high density (11.3 g/cm^3), providing a mass absorption coefficient of 2.2 cm^2/g at 140 keV associated with Tc-99m emission.

To obtain a better count rate performance, a reduction of collimator resolution cannot be avoided. On the other hand, collimators with better spatial resolution tend to reduce sensitivity at the cost of improving image details. Therefore, there is often a trade-off that should be made to the geometric dimensions of the holes and septa. The collimation system has an important role in spatial resolution, sensitivity, and count rate of acquired data; it affects the spatial properties and signal-to-noise ratio of the acquired scintigraphic images.

Different types and designs were proposed and operating in nuclear medicine laboratories. However, the general types of collimators used in nuclear medicine imaging are parallel hole, converging, diverging, and a special type known as a pinhole collimator, which has proved valuable in small animal imaging with superb intrinsic spatial resolution. The main differences among these types, as mentioned, are their geometric dimensions, including shape, size, and width of the collimator holes. Figures 10.2–10.4 show different types of collimators used in nuclear medicine clinics.

Parallel-hole collimators: The holes and septa of parallel-hole collimators are parallel to each other, providing a chance for those photons that fall perpendicular to the crystal surface to be accepted (Fig.10.2a). The image size projected by the parallel-hole collimator onto the crystal is 1:1 since it does not offer any geometric magnification to the acquired images. The most common types of parallel-hole collimator are

- Low-energy all-purpose (LEAP) (or low-energy general- purpose, LEGP) collimator
- Low-energy high-resolution (LEHR) collimator
- Low-energy high-sensitivity (LEHS) collimator
- Medium- and high-energy (ME and HE, respectively) collimators

a: Hole length

d: Hole diameter
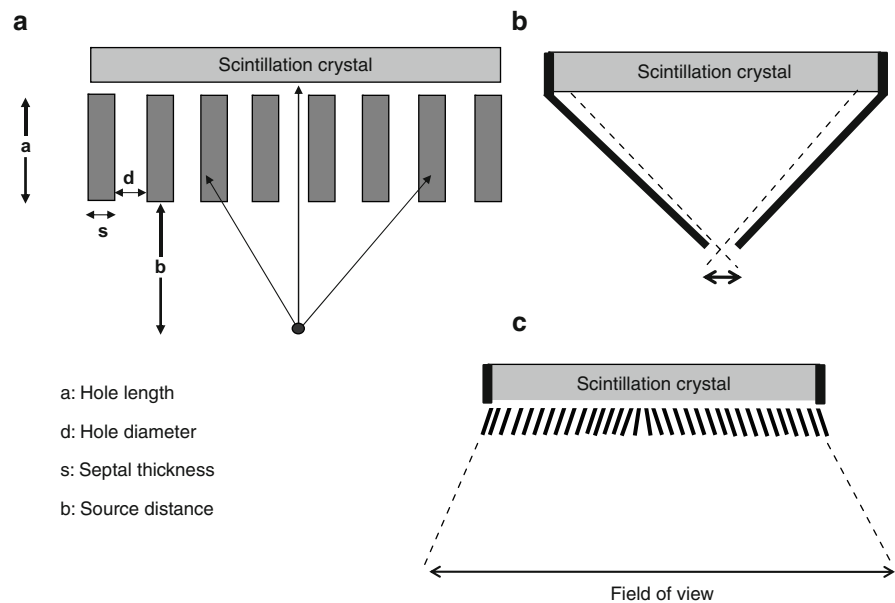
s: Septal thickness

b: Source distance

Fig. 10.2 Three different types of collimator. (**a**) Shows the parallel geometry along with definition of collimator holes and septa. (**b**) Pinhole geometry. (**c**) Divergent collimator

Fig. 10.3 Three different types of parallel-hole collimators: low-energy high-resolution, low-energy general-purpose, and low-energy high-sensitivity collimators. *FWHM* full width at half maximum
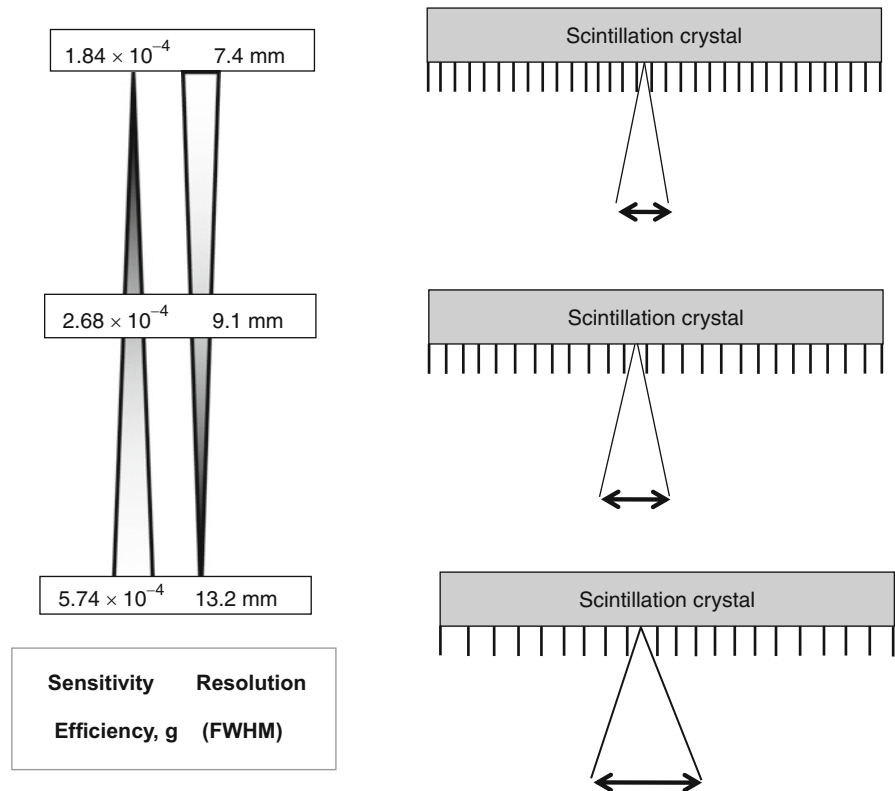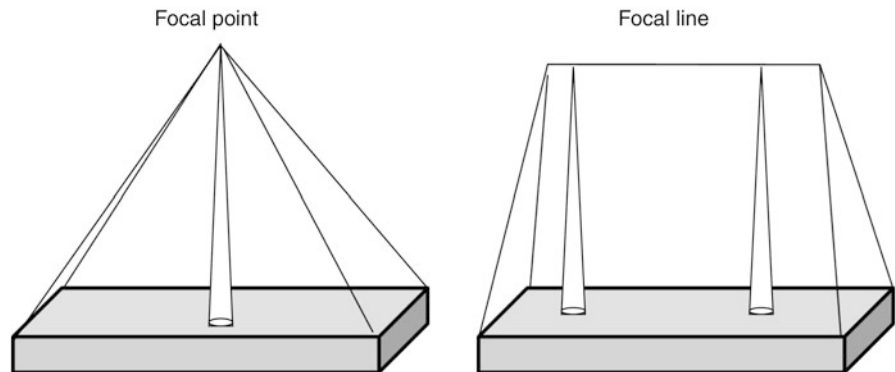
1.84×10^{-4}	7.4 mm
2.68×10^{-4}	9.1 mm
5.74×10^{-4}	13.2 mm

Sensitivity	Resolution
Efficiency, g	(FWHM)

Scintillation crystal

Scintillation crystal

Scintillation crystal

Focal point

Focal line

Fig. 10.4 Cone beam and fan beam collimators. For the former, all holes focus at a single point, while in the latter all holes at the same transaxial slice look at the same focal point

LEHR collimators provide a small acceptance angle by the aid of their narrow and longer holes. This helps to resolve fine details and improves the spatial resolution of the acquired images. Moreover, it tends to keep resolution at a distance and hence is recommended in cardiac SPECT imaging due to the varying distance of the heart from the surface of the detector.

For *LEGP collimators,* **the** hole diameter is relatively larger, and the acceptance angle is wider than for the high-resolution (HR) collimator. It provides greater sensitivity and lower spatial resolution characteristics as opposed to the LEHR collimator. LEGP collimators are useful in examinations that require a high count rate (e.g., dynamic studies) to improve sensitivity while spatial resolution is not so influential

to the interpretation of the images. Table 10.1 compares the general purpose (GP) and HR collimators for a commercially available gamma camera system [11].

The difference in geometric dimensions of the hole diameter and length in addition to the septal thickness of both collimators results in a significant improvement of the sensitivity of the GP collimator over the HR collimator with minimal loss in resolution measurements. In Table 10.1, notice that the GP collimator provides a count rate efficiency about 50% greater than that of the HR collimator. It should be pointed out that manufacturers have their own special designs and label them differently. Collimator specifications given, for example, to a GP collimator might be completely different from those given by another manufacturer to the same type of collimator [12].

LEHS collimators: This type of collimators provides good count rate capabilities and produces images with low statistical noise if compared with other collimators given the same acquisition time. However, this is achieved by trading off the resolution properties of the acquired images. In other words, the improvement in sensitivity is obtained at the cost of compromising the detectability of fine structures. Figure 10.3 shows the trade-off between spatial resolution and sensitivity in collimator design.

HE and ME collimators: Medium-energy radionuclides in nuclear medicine such as gallium-67 and In-111 and high-energy radionuclides such as I-131 and Fluorodeoxyglucose-F18 (FDG) have high penetrating power and thus could penetrate collimator septa, causing higher background images and could adversely affect spatial contrast. ME and HE collimators have increased septal thickness and provide a lower transparency to high-energy gamma photons than lower-energy collimators. However, radionuclide studies that use ME and HE collimators manifest lower spatial resolution by degrading small-size lesions. As a result, lower quantitative accuracy is achieved by partial volume averaging [13]. Nevertheless, ME collimators were recommended over LE collimators in studies that required low-energy photons (e.g., iodine-123) if there

were other emissions of higher-energy gamma rays to lessen septal penetration artifacts and improve quantitative accuracy. Some manufacturers overcame the problem by introducing new collimators with a special design that are able to maintain resolution and sensitivity of the examination while providing lower septal penetration [13].

Converging and diverging collimators have a field of view different from parallel-hole collimators with the same exit plane size. The converging collimators have a smaller field of view, whereas the diverging ones offer a larger field of view than that provided by parallel-hole collimators. In diverging collimators, the direction of the holes diverges from the point of view of the back surface of the collimator (the face opposing the crystal). They are used in cameras with a small field of view so that they can lessen large organs to be projected onto the camera crystal (Fig. 10.2c).

In *converging collimators*, the holes are converging from the perspective of the back surface of the collimator. Cone beam and fan beam are special types of gamma camera collimators; the former has one focal point for all collimator holes that lies at a certain distance away from the collimator surface and is called the focal point. The focal length is minimal at the center of the collimator and increases gradually as it goes to the periphery. In the fan beam collimator, each row of collimator holes has its own focal point, and all the focal points form a focal line for the entire collimator. As such, it has parallel collimation along the axial direction of the subject and converging collimation within each slice, providing independent and nonoverlapping projection profiles. This geometry allows for a simplified slice-by-slice image reconstruction to be applied. Cone beam geometry, however, complicates image reconstruction by involving the holes axially and transaxially. Both collimators are shown in Fig. 10.4.

A converging collimator provides a magnified view of small objects found at locations between the collimator surface and the focal point/line with relative improvement in count sensitivity, which is maximum at the focal site. They are of particular interest in brain

Table 10.1 Characteristics of two different collimators: low-energy general-purpose (GP) and high-resolution (HR) collimators[a]

Collimator	Hole diameter (mm)	Septal thickness (mm)	Hole length (mm)	Resolution at 15 cm (mm)	Relative efficiency
GP	1.40	0.18	25.4	11.5	1.0
HR	2.03	0.13	54.0	9.5	0.52

[a]Taken from Ref. [11].

tomographic imaging and in some other applications. Resolution of the converging collimator is maximum at the surface and decreases with an increase in source distance, while the sensitivity increases gradually from the collimator surface until the source reaches the focal point. This is because the fraction of holes that can see the object at a near distance increases with an increase in object distance; therefore, the object at larger distances is seen by more holes, resulting in improved sensitivity. Magnification takes place only in one direction, typically the transverse direction, and the cone beam collimator magnifies along the axial direction as well [14]. The drawbacks of converging collimators are reduced field of view and data insufficiency for 3D (three-dimensional) reconstruction.

Pinhole collimator: The pinhole collimator is an important type that is used frequently in nuclear medicine laboratories, especially in small-organ imaging, such as thyroid and parathyroid scanning (Fig. 10.2b). Also, it has useful applications in skeletal extremities, bone joints, and the pediatric population. It is a cone-shaped structure made of lead, tungsten, and platinum and has an aperture of a few millimeters in diameter (2–6 mm). In the small-animal pinhole collimator, the aperture size can go decrease to 1–2 mm or even less to meet the resolution requirements imposed by small structures and minute tracer uptake [15]. The collimator length that extends from the back surface to the point of the aperture is 20–25 cm. Image formation can be described using lens equations in the sense that the acquired data reveal an inverted and magnified image. The pinhole collimator provides a magnified image of small objects, yielding an appearance that reflects an improvement in spatial resolution.

10.2.3 Crystal

Scintillation crystal is the second component that encounters the incident photons after passing the collimator holes. There are some favorable properties based on which the crystal needs to be selected before implementation in gamma camera design. Scintillators of high density, high atomic number, short decay time, high light output, and low cost are desired and allow better imaging performance. However, there is no ideal detector material in the field of diagnostic radiology; most often, the selected material has some

Table 10.2 Properties of scintillation crystals used in gamma camera

	Na(Tl)	CsI(Tl)	CsI(Na)
Z_{eff}	3.67	54	54
Density (g/cm^3)	50	4.51	4.51
Decay time (ns)	230	1,000	630
Photon yield (keV)	38	45–52[a]	39
Refraction index	1.85	1.8	1.84
Hygroscopic	Yes	Slightly	yes
Peak emission (nm)	415	540	420

[a]CsI(Tl) is poorly matched to the response of photomultiplier tube (PMT). However, the scintillation yield is much higher when measured by photodiodes with extended response into the red region of the spectrum [20].

desired features that make it preferred over alternatives. Table 10.2 lists the most common crystals used in gamma camera design.

The most commonly used detector material for the gamma camera is the thallium-activated sodium iodide [NaI(Tl)] crystal. It utilizes the scintillation phenomenon to convert gamma rays into light quanta that can be amplified by a PMT to produce a detectable electronic signal. Scintillation occurs when the incident photon interacts with the crystal material to produce photoelectrons or Compton scattering. The resulting electrons from photoelectric or Compton interactions travel short distances within the crystal to produce more interactions in a form of excitations or ionizations of the crystal atoms and molecules. These excited products are deexcited by converting to the ground state by releasing scintillation light.

A continuous large slab of sodium iodide crystal is the conventional structure that is used in most gamma camera designs. The crystal thickness can be 3/8 in., 5/8 in., or even larger for high detection efficiency [16]. A pixilated or segmented version of scintillation crystals has also been utilized in small SPECT systems using photosensitive PMTs as photodetectors and parallel or pinhole imaging geometry, yielding high-resolution tomographic images. Segmentation of the scintillation crystal allows the spatial resolution of the imaging system to be improved to an extent determined mainly by the segmentation size. Nevertheless, this comes with a reduction of count sensitivity, increased costs, and degraded energy resolution [17]. It is often used in small field-of-view, organ specific-systems or in small-animal scanners. Another option

that can be considered as an intermediate solution between continuous and segmented or pixilated crystals is partially slotted crystals, which have been investigated to produce better energy resolution than fully pixilated crystals and improved detection sensitivity while maintaining the spatial resolution at better levels with an appropriate data analysis [18, 19]. Additional features provided by such systems are their relative ease and cheap manufacturing costs.

The NaI(Tl) crystal is formed by adding a controlled amount of thallium to a pure sodium iodide crystal during growth. The addition of thallium makes the NaI crystal scintillate at room temperature since pure a NaI crystal works at a low temperature under nitrogen cooling [9, 20]. Some precautions are taken into account during the design of the NaI(Tl) crystal. It must be sealed in an airtight enclosure, usually aluminum, to avoid exposure to air owing to its hygroscopic properties. Exposing the crystal to air can cause yellow spots, which can develop heterogeneous light transmission.

Thallium-activated cesium iodide, CsI(Tl), is slightly denser than sodium iodide crystal and better suited if coupled to photodiodes as the emission wavelength is shifted to higher values, at which the response of PMTs is relatively weaker. It therefore does not properly fit the requirements imposed by PMTs, which need light quanta of shorter wavelengths. A pixilated CsI(Tl) crystal has been tested in a miniaturized gamma camera with the collimator matching the detector array and size suitable for breast imaging. The system showed good performance characteristics, such as an improved spatial resolution, high detection efficiency, and better scatter rejection (~8% full width at half maximum [FWHM] at 140 keV) [21]. The CsI(Tl) crystal has also been utilized in a pixilated fashion and coupled with silicon photodiode in a commercial design developed as a dedicated cardiac tomograph. Cardius 3 XPO is manufactured by Digirad and consists of 768 pixilated Cs(Tl) crystals coupled to individual silicon photodiodes and digital Anger electronics for signal readout [22].

Sodium-activated cesium iodide, CsI(Na), has an emission spectrum similar to NaI(Tl) that suits PMT response, with comparable light yield and relatively slow decay time. It has been utilized in small-animal SPECT scanners in pixilated 5-mm thickness (21 × 52 pixels of 2.5 × 2.5 mm) coupled to photosensitive PMTs [23]. The system provided an intrinsic spatial resolution of 2.5 mm, intrinsic energy resolution of 35% (at 140 keV), and intrinsic sensitivity of 42% using an energy width of 35% at 140 keV. Comparison of partially slotted CsI(Na) and CsI(Tl) crystals revealed the superior performance of the latter in terms of detection efficiency and spatial and energy resolution [19].

Yttrium aluminum perovskite (YALO3:Ce) is a nonhygroscopic scintillation crystal with the structure of the perovskite and is called YAP. It has a density of 5.37 g/cm^3, an effective atomic number of 34–39, and light output of 40% relative to NaI(Tl) and is used for gamma as well as annihilation coincidence detection [24]. Lanthanum bromide (LaBr:Ce) is a fast scintillator (short decay time, 16 ns) with high light output. These characteristics are suitable for time-of-flight applications in PET scanners (see Chap. 11). High light yield is an important parameter that improves the certainty of photon statistics and serves to improve system spatial and energy resolution. The crystal has been evaluated using a flat-panel, photosensitive PMT; it showed good imaging performance for single-photon applications with superior energy resolution (6–7.5%) and spatial resolution of 0.9 mm. The detection efficiency was also high, yielding 95% at 140-keV photon energy [25–27].

While SPECT and PET can be combined into one imaging device known as hybrid SPECT/PET camera, there are some modifications that have to be implemented in electronic circuitry and crystal thickness. The latter should be adapted to improve photon detection efficiency. The NaI(Tl) crystal is an efficient scintillator for low-energy photons; it is greater than 95% for 140 keV. However, its response against 511 keV is significantly poorer as it shows a coincidence detection efficiency of about 10%.

Some manufacturers have used the traditional scintillation crystal by increasing the thickness up to 25 mm, while others have modified the crystal so that the back surface of the crystal is grooved, allowing detection of single-photon emitters to be maintained. Meanwhile, the system is efficiently able to image patients injected with medium- and high-energy radiotracers. However, all the major suppliers are currently providing PET scanners with a more efficient performance, which have a cylindrical-type design.

StarBrite crystal, developed by Bicron Corporation (Newbury, OH), is a dual-function 1-in. thick crystal that serves to improve the detection efficiency of

medium- and high-energy photons and has been incorporated in some commercial designs [16, 28] (see Fig. 10.5). The slots at the back surface of the NaI(Tl) crystal are machined to prevent light diffusion, reducing the impact of wide-angle reflected light. This also maintains a uniform light collection as a function of position, achieving better intrinsic spatial resolution (4 mm) [29, 30]. In performance evaluation with other systems, this design provided a good compromise in terms of spatial resolution and sensitivity for ^{111}In ProstaScint® SPECT imaging. However, the

collimator-crystal pair combined with system electronics work together to determine the overall system spatial resolution and sensitivity given a particular detection task.

In humans, visual perception is the ability to interpret information and surroundings from visible light reaching the eye. In a similar way, the light released from the scintillator after the interaction of the incident radiation with the detector system needs an interpretation process. This process in the gamma camera is implemented by the readout component or photodetectors that lie in close proximity to the back surface of the scintillation crystal. A remarkable feature of the design made by Anger is the photomultiplier mapping of the detector crystal together with the mathematical logic he used in event identification.
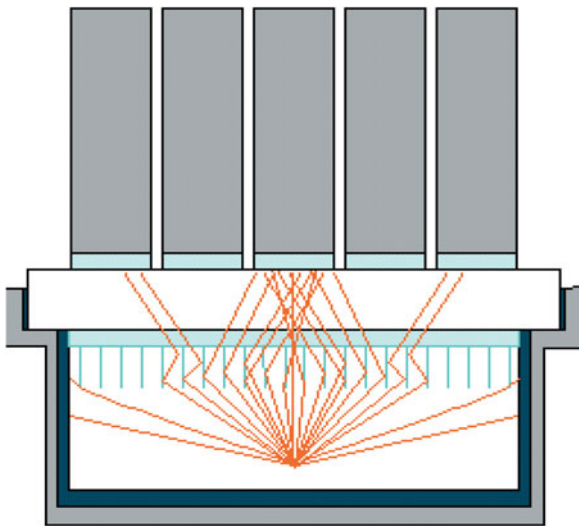

Fig. 10.5 StarBrite. (Courtesy of Saint-Gobain Crystals)

10.2.4 Photomultiplier Tube

The PMT is an important hardware component in the detection system of the gamma camera. Its main function is to convert the scintillation photons to a detectable electronic signal. The PMT as shown in Fig. 10.6 is a vacuum tube consisting of an entrance window, a photocathode, focusing electrodes, electron multiplier (dynodes), and anode. The PMT has a long history in many applications, including medical as well as other fields such as high-energy physics, spectrophotometry,
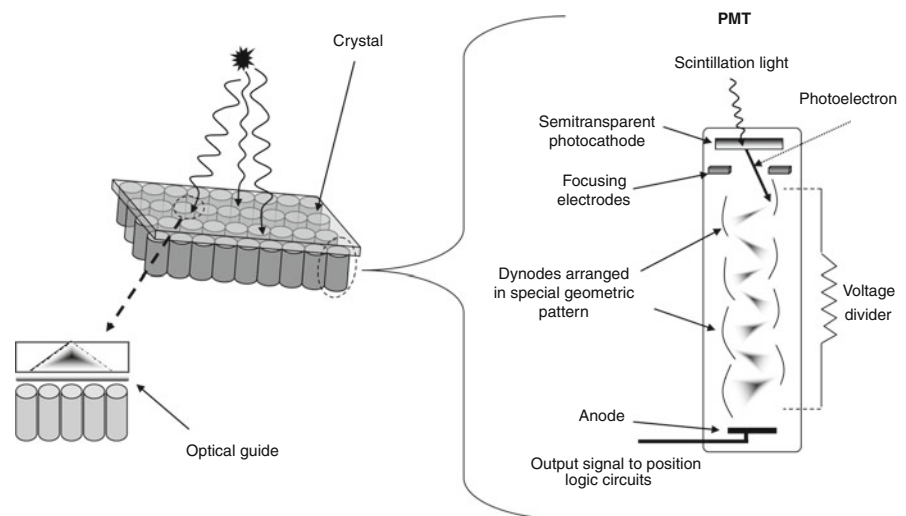

Fig. 10.6 Photon interaction and conversion to electronic signal

and is widely used in many SPECT and PET imaging systems.

10.2.4.1 Photocathode

The photocathode is a photo-emissive surface usually consisting of bialkali metals with low work functions and weakly bound valence electrons. The photocathode receives the scintillation light from the crystal, such as an NaI(Tl), by a wavelength of 415 nm at maximum. The material for the photocathode that emits photoelectrons (on an incidence of light quanta) equivalent to that wavelength will be the material of choice as it will allow increasing the amount of electrons emitted and hence will be able to improve the certainty of the output signal [31].

The photons emitted from the NaI(Tl) crystal fall on the photocathode of the PMT to eject photoelectrons by the physical phenomenon of photoelectric effect. The emitted electrons are amplified through a series of dynodes placed in a special geometric pattern with high potential difference so that each dynode has greater voltage (100–300 keV) than the preceding one. When scintillation light strikes the photocathode, it releases electrons, which are accelerated by the effect of the high voltage on the first dynode to collide with it. Electrons emitted from the first dynode are accelerated to the second dynode to eject more electrons on collision. The third dynode accelerates the electrons from the second dynode toward its face; this multistage electron amplification continues until the electrons reach the last dynode. At the back end of the PMT, the anode of the PMT collects all the electrons that result from this cascade process. Figure 10.6 illustrates the process of photon conversion to electronic signal after interaction with the crystal.

10.2.4.2 Anode

The anode of the PMT is an electrode that collects the amplified electrons through the multistage dynodes and outputs the electron current to an external circuit. An adequate potential difference between the anode and the last dynodes can be applied to prevent space charge effects and obtain a large output current [32]. PMTs have a large electronic gain that can reach 10^6–10^8 in addition to low electric noise. However, the *quantum conversion efficiency* of PMT is low since, on average, for every ten scintillation photons that fall on the photocathode, there is approximately a release of two electrons, resulting in an efficiency of about 20–25% [29]. This in turn has an impact on intrinsic spatial resolution and energy resolution. The PMT is susceptible to variations in high-voltage power supply, and its performance is influenced by temperature, humidity, gravity, and magnetic field because of the high voltage applied on the dynodes (a limitation in design of PET/MRI scanners).

10.2.5 Preamplifier

The shape of the output signal from the PMT is a rapid rising peak with a slow decaying tail. The rapid peak denotes the decay time of the scintillation event within the crystal, and the decaying tail denotes the time taken by the electrons to traverse the PMT. The output signal of the PMT cannot be fed directly into the amplifier because of the impedance difference between the PMT and the amplifier. The preamplifier plays an important role in this regard. It matches the impedance between the PMT and the main amplifier so that it could be handled by the amplifier and other subsequent electronics. The function of the preamplifier is matching, shaping, and sometimes amplification of the signal [9].

Matching: The signal produced from the PMT has a high impedance value, and this requires matching with the other electronic circuit components, (i.e., amplifier).

Shaping: The signal that is to be fed into a main amplifier needs to have a certain pulse decrease time to allow proper pole-zero and baseline correction. The preamplifier works to shape the PMT signal using an resistor-capacitor circuit (RC) by increasing the time constant, which is then handled by the amplifier.

Amplification: The amplification element of the preamplifier varies in the amount of amplification according to the type of detector and the magnitude of the signal. In PMT electronic assembly, the preamplifier sometimes has no significant amplification gain since the PMT itself provides a considerable amplification through the multistage process of the dynodes. The output signal from the preamplifier is a slow

decaying pulse that causes pulse pileup. However, it conveys information regarding the signal amplitude and timing of the scintillation event. This information requires more additional manipulation by an amplifier without introducing any type of distortion. The newly developed SiPM (silicon photomultiplier) photodetectors (discussed in a separate section of this chapter) provide similar amplification gain as that of PMTs; hence, preamplification requirements are less demanding in comparison to photodetectors with low gain properties.

10.2.6 Amplifier

The amplifier plays a major role in signal amplification and shaping; it is therefore called a shaping amplifier. Signal amplification is required to permit further processing by the rest of the detector electronics. However, the amplification factor varies greatly with application and typically is a factor of 100–5,000 [20]. Shaping of the signal is accomplished by eliminating the tail from the output signal and giving each signal its separate width and amplitude without overlapping with other signals. In summary, the functions of the amplifier are shaping the pulse and decreasing the resolving time and providing higher gain to drive PHAs, scalars, and so on. It also provides stability to maintain proportionality between pulse height and photon energy deposition in the crystal. The amplifier serves to increase the signal-to-noise ratio and maintain proper polarity of the output signal [33].

10.2.7 Pulse Height Analyzer

There are different probabilities for the interaction of the incident gamma radiations with the crystal. Some photons impart a fraction or all of their energy into the crystal, whereas other photons impart some of their energy and escape the crystal without further interactions. Another fraction of photons undergo more than one interaction, dissipating all their energies. Therefore, there are two general forms of scatter that serve to reduce the capability of the system to accurately determine the position and the energy of the incident

gamma radiations. One part results from scattering that takes place inside the patient body, and the other part results from scattering that occurs in the camera crystal. The latter is not significant and does not contribute to a great extent to the total fraction of scattered radiation and the shape of the pulse height spectrum. It is important in medium- and high-energy gamma photons (e.g., In-111 and ^{131}I) and in thick crystals. The former type of scattering dominates the spectrum and results in degraded image quality and contrast resolution. As a result and for other instrumental reasons (e.g., detector energy resolution), the output signal is not a sharp peak line on the spectrum; it is a distribution of pulse heights with one or more photo peaks representing the energies of the administered radionuclides. The output signal is measured in terms of voltage or "pulse height," and every pulse has amplitude proportional to the amount of energy deposited by the gamma ray interactions. A pulse height analyzer (PHA), as the name implies, is a device that that is able to measure the amplitude pulse heights and compare them to preset values stored within it. There are two types of PHA: single channel and multichannel.

10.2.7.1 Single-Channel Analyzer

The single-channel analyzer records events within a specified range of pulse amplitude using one channel at a time, applying lower and upper voltage discriminators. The output signal of the amplifier has a range of heights (voltages), and selection of the desired signals for counting is achieved by setting the lower discriminator to a level that diminishes all lower amplitudes, thereby allowing the upper values to be recorded.

10.2.7.2 Multichannel Analyzer

Acquisition studies that require more energies to be detected, as in dual-radionuclide acquisitions (e.g., parathyroid Tl-201–Tc-99m subtraction, meta-iodobenzylguanidine(MIBG)-131–Tc-99mDTPA [diethylenetriaminepentaacetate], and others) and radionuclides with more than one energy photo peak (e.g., Ga-67, In-111, and Tl-201), the proper choice for recording these energies separately and simultaneously is to use a

multichannel analyzer (MCA). An MCA provides a means of rejecting the scatter region from the spectrum, allowing the acquired image to be less contaminated by scattered photons. However, the photo peak region will still contain a significant fraction of photons that have undergone small-angle scattering. The MCA allows an energy window to be set over the photo peak centerline to confine the accepted photons to a certain energy range. This range is chosen by lower and upper voltage discriminators. The former determines the threshold below which all pulse heights are rejected, and the latter determines the value at which no higher values are accepted. Values that fall between the lower and upper discriminator are adjusted by a window width and often are a percentage of the photo peak energy. For example, a 20% energy window is usually selected over the 140-keV photons emitted by Tc-99m. A 15% window is also used with an improvement in contrast and minimal loss in primary photons. Moreover, a 10% window is used at the expense of reducing sensitivity [34]. An asymmetric window is another way to reduce the effect of scattered photons as it can improve image contrast, spatial resolution, and clinical impression [35, 36].

A variety of scatter correction techniques has been devised to reduce the adverse effects of scattered radiation. For proper quantitation and absolute measures of tracer concentrations, images must be corrected for scatter and other image-degrading factors. A gamma camera with an MCA is necessary when energy-based scatter corrections are applied to the acquired data. Advances in semiconductor technology have motivated the development of gamma camera systems with significant improvement in energy resolution. This in turn improves the spatial contrast and signal-to-noise ratio, resulting in improved image quality. Chapter 15 has more details about the scatter phenomenon and its correction techniques.

10.3 Other Photodetectors

10.3.1 Position-Sensitive PMT

The position-sensitive PMT (PSPMT) is a modified version of the conventional PMT but with compact size and position determination capabilities, allowing for an improvement in image spatial resolution. The PSPMT-based gamma camera shows the same advantages of a standard gamma camera with the additional possibility of utilizing scintillation arrays with a pixel dimension less than 1 mm, thus giving the ability to achieve submillimeter spatial resolution [37]. Several models have been developed since its introduction in 1985 [38]. Three different types can be found [39, 40]:

Proximity mesh dynode: This is the first generation and is based on the proximity mesh dynode, by which the charge is multiplied around the position of the light photon striking the photocathode. The charge shower has a wide intrinsic spread. This model can provide a large active area (e.g., 5 in.) and large number of dynodes (e.g., 256) but with large dead space.

Multichannel dynode: This is a multianode structure that minimizes cross talk between anodes and provides better localization measurements. This type has the following drawbacks: large dead zone, limited effective area, and limited number of dynodes.

Metal channel dynode: Combined with multichannel or crossed-plate anode techniques, this dynode can provides low cross talk and well-focused charge distribution, reducing the intrinsic spread to 0.5 mm FWHM [39]. For SPECT imaging, the use of a crossed-wired anode PSPMT is more suitable when coupled with a flat crystal because of continuous position linearity requirements. However, this configurations may not allow the best performance of the PSPMT; thus, to utilize the full potential of its intrinsic characteristics, a multicrystal array is needed to attain high detection efficiency, narrow light spread function, and reasonable light output [41].

A PSPMT is relatively more expensive than the conventional type, and most of its use is in preclinical small-animal SPECT and PET scanners and portable and compact miniaturized gamma cameras, and it is of interest in producing high-resolution breast scanners [42, 43]. This type of diagnostic examination requires compact and flexible systems to fit geometric requirements imposed by the female breast. The technologic advances in the development of a compact flat-panel PSPMT with less dead space allowed manufacture of a portable gamma camera with a large detection area and high imaging performance with better spatial resolution [44]. It has become possible that an array of 256 crystal elements can be coupled directly to one PMT, and the crystals can be read out individually [45].

Fig. 10.7 Hamamatsu H8500 flat-panel position-sensitive photomultiplier tube (PSPMT). (From [100]. © 2006 IEEE with permission)

The Hamamatsu H8500 flat-panel PSPMT is shown in Fig. 10.7.

10.3.2 Avalanche Photodiode

An interesting trend is the development of semiconductor photodetectors to replace the bulky and significantly large volumetric shape of the PMT. One of the major drawbacks of PMTs is their sensitivity to magnetic fields. As the electrons are accelerated within the PMT by the effect of high potential applied between photocathode and dynodes and between successive dynodes, any source that influences this process would be an undesired component of noise leading to tube performance degradation. A magnetic field more than 10 mT is able to alter the gain and energy resolution of a PMT [46]. One of the earliest solutions was to use long cables of fiber optics. The better alternative was then to use semiconductor photodetectors. Efforts have been made to develop semiconductor detectors with better detection efficiency and intrinsic spatial resolution, providing a reliable and robust performance compared to PMTs or PSPMTs. Among these developments are the avalanche photodiodes (APDs), which can be produced in small dimensions, providing an improvement of spatial resolution in addition to reduced detector volume, and thereby fit space requirements imposed by multimodality imaging scanners. They are also well suited for pixilated

detectors and crystals of longer wavelengths, such as mentioned for CsI(Tl) crystals. They have higher gain than silicon photodiodes and better timing characteristics, on the order of 1 ns [47].

In comparison to the PMT, the APD is sensitive to temperature variations, can be operated in a lower voltage than a PMT, and is stable in the presence of high magnetic fields, like that encountered in MRI [48]. Thus, the APD was suitable in PET inserts incorporated into MRI machines, providing compact and simultaneous hybrid PET/MRI imaging systems. The semiconductor junction is operated at a high reverse bias, and the output signal is proportional to the initial number of light photons. They are characterized by low gain and relatively higher quantum efficiency.

The *position-sensitive APD (PSAPD)* is similar to the APD but with fewer readout requirements. The back surface is connected to a resistive layer that allows for multiple contacts to be fabricated. Position information can then be obtained by the charge sharing among electrodes that enables the determination of position of interaction [49]. Consequently, this structure allows for simple and compact detector assembly and enables use of significantly fewer readout channels, resulting in lower manufacturing costs. The alignment of the detector with the crystal array in this design is not as important as is the case in the individual APD array. This type of photodetector has an attractive interest in small-animal scanners, including depth of interaction encoding, to improve scanner spatial resolution and sensitivity [50–52]. This type also has applications in high-resolution small-animal imaging systems. For example, it has been coupled to a CsI(Tl) scintillator in a multipinhole small-animal SPECT system with significant improvement in detection efficiency and spatial resolution on the order of 1 mm [53].

10.3.3 Silicon Photomultiplier

The Geiger-mode APD or silicon photomultiplier (SiPM) is a densely packed matrix of small APDs $(20 \times 20\text{–}100 \times 100~\mu m^2)$ joint together on common silicon substrate and work in limited Geiger discharge mode. Each cell is an independent Geiger mode detector, voltage biased, and discharges when it interacts
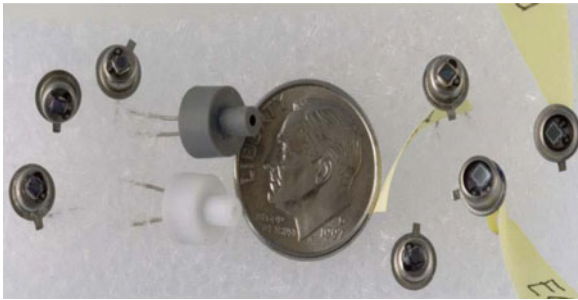
Fig. 10.8 Silicon photomultipliers (SiPMs) from different manufacturers. (From [101]). © IEEE with permission)

with an incident photon. The scintillation light causes a breakdown discharge for triggering a cell resulting in a fast single photoelectron pulse of very high gain 10^5–10^7. SiPM produces a standard signal when any of the cells goes to breakdown. When many cells are fired at the same time, the output is the sum of the standard pulses [54]. Characteristics of SiPM are low noise factor, photon detection efficiency equivalent to the standard PMT, and low bias voltage. The higher gain feature provided by SiPM detector marginalizes the electronic noise in contrast to the standard APDs, which generally have a gain of 100–200. However, the dead space around each pixel and the finite probability of photons to produce avalanche breakdown reduce the detection efficiency of the SiPM, making it significantly lower than for the APD [55]. An SiPM is an interesting alternative to the conventional PMT in terms of compactness, same level of electronic gain, suitability for PET inserts in magnetic resonance systems and in detector design based on depth encoding information [56, 57]. Figure 10.8 shows SiPMs from different manufacturers.

10.4 Semiconductors

Instead of detecting the scintillation light on multiple stages, semiconductor detectors provide a detection means by which the incident radiation is converted to an electronic signal once it interacts with the detector material. The standard gamma camera, however, relies on converting the incident photon to a scintillation light, which is then amplified through a multistage

process in the vacuum of the PMT to yield an amplified signal that afterward is used in the calculation of event position and energy.

The use of semiconductor material in the field of radiation detection and measurements has been established for many years in different areas of science and engineering. The most commonly used are silicon (Si) and germanium (Ge). The atomic number of the former is 14, while for the latter it is 32; incorporating them in a radiation detector necessitates cooling to liquid nitrogen temperatures to avoid electronic noise generated from excessive thermal effects [58]. To fabricate a gamma camera based on a semiconductor detector, there has been efforts to search for other materials of high detection efficiency and amenable for operation in a room temperature environment.

Better alternatives of interest in the design of gamma ray detection systems are cadmium telluride (CdTe) and cadmium zinc telluride (CdZnTe), which can be considered promising materials for radiation detectors with good energy resolution, high detection efficiency, and room temperature operation. Several advantages can be obtained when designing a gamma camera based on semiconductor detectors. One is system portability as they enable construction of a compact structure free from the PMT and its bulky volume. A semiconductor camera also provides improved image contrast due to its better energy resolution compared to a sodium iodide crystal. Besides this last feature, high spatial resolution images can be obtained owing to the pixilated structure that can be implemented in the detector design [59].

More than one commercial SPECT system has been released to the market making use of semiconductor technology for improving imaging quality and diagnostic accuracy. D-SPECT (Spectrum Dynamics) is a CZT-based semiconductor camera commercialized for imaging cardiac patients. The system consists of nine collimated detector columns arranged in a curved configuration to conform to the shape of the left side of a patient's chest. Each individual detector, which consists of 1,024 (16 × 64) 5-mm thick CZT elements (2.46 × 2.46 mm), is allowed to translate and rotate independently so that a large number of viewing angles can be achieved for the region of interest [60]. The improved energy resolution (5.5% at 140 keV) also allows simultaneous application of a dual-isotope protocol with better identification of lesion defect and reduction of photon cross talk [61, 62]. Another design

has been introduced by GE Healthcare (Discovery NM 530c) that utilizes an array of pixilated (CZT) semiconductor detectors in fixed positions (without motion) that allow acquisition of cardiac projections in a simultaneous manner. Preliminary evaluations of the system demonstrated an improvement in image spatial resolution, energy resolution, and sensitivity as opposed to a conventional gamma camera design [63]. An additional feature was brought about by combining this system with CT in an integrated SPECT/CT (Discovery NM 530c with the LightSpeed VCT or Discovery NM/CT 570c) system.

A semiconductor camera made of CZT is relatively expensive; thus, most of the current commercial versions are confined to handheld, miniaturized imaging systems or intraoperative small probes. Scintimammography is one of the diagnostic procedures that requires a dedicated device able to match the position and geometry of the breast. Small and deep lesions are a challenging task and require characteristics better than provided by a standard gamma camera. The sensitivity of the test is limited by the lesion size, particularly for those less than 10 mm [64].

The difficulty in detecting small and deep pathologic breast lesions by conventional imaging systems lies in their limited detection efficiency and relatively poor spatial resolution. However, earlier detection of a breast lesion has better diagnostic and prognostic implications. This in turn should be met by instruments with high performance characteristics that provide better lesion detectability. A breast imager based on semiconductor materials such as CZT can provide better spatial and energy resolution, leading to improved lesion contrast. This can be achieved using a narrow energy window, reducing the adverse effects of scattered photons on image quality. Another property of the semiconductor camera is its compactness, portability, and smaller dimensions, which fit well with breast imaging [65–67].

10.5 SPECT/CT

Nuclear imaging using SPECT or PET techniques have well-known capabilities in extracting functional and metabolic information for many human diseases. The anatomical details provided by CT and MRI enjoy better structural description for human organs by resolving capabilities that are significantly higher than that provided by nuclear SPECT and PET machines. They have the advantages of providing a resolution in the submillimeter range, precise statistical characteristics, and better tissue contrast, especially in the presence and use of contrast media [68]. However, it lacks the property of describing the functional status of a disease. This is important in following up cancer patients postsurgically and in the presence of fibrotic or necrotic lesions after chemo- or radiotherapy [69].

The early work of Hasegawa and colleagues opened a gate to many applications in the field of diagnostic radiology and nuclear medicine by coupling two imaging techniques into one operating device: The SPECT camera has been merged to x-ray computed tomography (CT) in the same device to provide an inherent anatomolecular imaging modality able to depict morphological as well as functional changes in one imaging session. While this process of image coregistration can be accomplished by fusing images obtained from two separate modalities, it has been demonstrated that inline SPECT or PET and CT image acquisition would be more advantageous.

The advantages provided by CT to functional imaging are not singular. It enables the reading physicians to precisely localize pathological lesions detected on functional images with great confidence. The other advantage is the improvement in performing attenuation correction. Again, although this can be performed by radionuclide transmission sources, the CT-based attenuation correction has been shown to outperform radionuclide-based transmission scanning by providing fast and significantly less-noisy attenuation maps.

Another benefit provided by CT is the capability of deriving dosimetric measurements from the fused images due to accurate outlining of the region of interest and thus better volumetric assessment. In the field of nuclear cardiology, SPECT/CT systems are of particular importance due to the continuous debate about attenuation correction [70, 71] and other degrading factors that reduce diagnostic quality and quantitative accuracy, such as partial volume effects [72]. Apart from attenuation correction, calculation of calcium scoring is also possible with the CT portion of the machine in addition to performing noninvasive coronary angiography.

In some instances, the addition of CT data to the functional images provides a guiding tool for

image-based biopsy and thus can play a role in patient management; it also can be of synergistic effect in radiotherapy treatment planning, targeted treatment with brachytherapy, or intensity-modulated radiation therapy [73]. However, this has become more attractive with PET imaging than SPECT derived data.

The image of the year for 2006 was an SPECT/CT image showing both the coronary arteries and blood flow to the heart. This took place at the 53rd annual meeting of the Society of Nuclear Medicine in San Diego, California. The images clearly depicted the anatomical correlation of the blood flow defects to the corresponding artery. SPECT/CT devices also are of interest in preclinical and molecular imaging research with similar benefits as those provided to the clinical arena in addition to increased flexibility in performing longitudinal research studies.

On the research level, a tremendous improvement in the spatial resolution of micro-CT systems has enabled the investigators to look at minute structural changes that were not possible to see with conventional systems. Advances in micro-CT systems has revealed images of 10 μm and far better, permitting subcellular dimensions to be imaged [74].

10.5.1 Levels of Integration

Transmission scanning has been defined as "a useful adjunct to conventional emission scanning for accurately keying isotope deposition to radiographic anatomy" [75]. This article was published by Edward and coworkers in the mid-1960s when they realized the importance of combining functional data with their anatomical templates, although they used a simple approach to obtain the transmission scanning. Investigators assigned this as the first demonstration of the feasibility of hybrid imaging [76]. They used an Am-241 source located at the center hole of a collimated detector; the other detector was adjusted to acquire the emission and transmission data. This early functional/anatomical study is a clear sign of the early recognition of combining the two types of images to strengthen each other and to overcome their inherent weaknesses. However, despite this interesting beginning, it was not pursued, and both imaging modalities were almost developed independently until the early 1990s. Before this time, there was some interest

and research efforts to use radioactive transmission sources for attenuation correction [77, 78]. The approaches and different levels of integrating structural imaging with the functional data were as follows:

1. The *primitive level* of integrating functional and structural images is evidenced by the human brain. This is the traditional way that diagnosticians used to correlate two images acquired from separate imaging modalities. However, human spatial perception and differences in image textures acquired from two different modalities represent a challenge for the reading physicians to mentally correlate the two data sets. This can be more problematic in small-size lesions and in identifying the spatial extent and spread of a disease.

2. The second level of image coregistration was brought to the clinic by software algorithms. They are relatively simple to apply to rigid structures such as the brain, where images acquired by CT or MRI can be merged to functional images acquired and processed on a separate SPECT or PET machine. This successful implementation is due to brain rigidity, and variations in the position of internal structures are less likely to occur compared to lung or abdominal image fusion. In a review [79], localization of brain structures was less challenging compared to whole-body applications, and image fusion may be required for only a subgroup of patients. Moreover, in a wide comparison of various available software tools for retrospective registration of PET/MRI and PET/CT, an accuracy of 2–3 mm was consistently achieved, which was below the voxel dimension of PET [80] and SPECT as well.

3. Use of intrinsic landmarks or extrinsic markers to accurately fuse the two data sets has been implemented with some impractical drawbacks placed on its feasibility in the clinical routine, added technical complexity to the diagnostic procedures, or inaccurate image correlation. This could arise from variations that may exist between imaging sessions, fixation strategy, or perhaps inability to correlate internal organs with external markers [69]. Furthermore, automatic registration for internal landmarks could also be affected by the limited spatial resolution of nuclear images with precise selection of anatomical landmarks; therefore, accurate alignment is not guaranteed. These apparent shortcomings of

image coregistration, particularly in nonrigid body structures, have motivated the development of non-linear 3D image fusion algorithms able to improve the accuracy of alignment.

4. Ideally, one would like to acquire the structural as well as the functional data in a simultaneous manner in the same spatial and temporal domain. This can be achieved when the detector systems can be incorporated into each other, achieving concurrent image acquisition. This multimodality design has been realized in hybrid PET/MRI systems with substantial modification to the PET detector system using APDs instead of the conventional PMTs, as mentioned in this chapter (see [81]).

5. The other alternative is to modify the detector technology so that a single detector system can record the two signals with adequate distinction for each individual electronic pulse. However, x-ray detector systems are energy integrators and do not allow individual events to be discriminated according to their energies. This is in great part due to the high fluence of the x-ray source compared to nuclear photon emission and owing to beam polychromaticity [82]. In other words, the significant differences in photon rates pose challenges to implement multimodality imaging using a "conventional" detector for both x-ray and radionuclide processes; this requires a detector that can switch between pulse-mode SPECT/PET acquisition and charge integration mode [83]. Nevertheless, it has been proposed to simultaneously acquire trimodality images, namely SPECT/PET/CT, with great complexities placed on detector design [84]. Moreover, an emerging technology is evolving to record both types of data in a single counting and energy integrator modes.

6. The other strategy is to place the two detector systems side by side such that images can be acquired in a sequential manner. This is the way all clinical SPECT/CT as well PET/CT scanners are presently manufactured and operated. Therefore, one can simply deduce that the higher the level of integration, the more demands placed on the technologic complexity. The range of multimodality imaging has been extended to include functional only, structural only, or a combination of functional and structural imaging modalities to yield a variety of integrated or hybrid diagnostic options [85] SPECT/CT is among the best

dual-modality approaches that drew the attention of many researchers in the field, and its technical value has been proven in a significant number of clinical conditions, leading to a change in patient management. Although other multimodality imaging approaches have been or are being developed, they are aimed most of the time toward preclinical imaging, and their clinical counterparts are yet to be determined.

10.5.2 Early and Recent SPECT/CT Systems

As mentioned, the work of SPECT/CT was launched and pioneered by Hasegawa and colleagues at the University of California, San Francisco, by designing the first prototype imaging system able to acquire both single-photon emitters and x-ray transmission scanning in one imaging session. The detector material was a high-purity germanium (HPGe) designed for simultaneous acquisition of functional and anatomical information. The system was a small-bore SPECT/CT system with some technical limitations for direct application in the clinical setting. The same group then developed a clinical prototype SPECT/CT system using a GE 9800 CT scanner and GE X/RT as the SPECT component mounted in tandem with data acquired sequentially using the same imaging table.

The industry recognized the potential of combining the two imaging techniques, and the first commercial SPECT/CT system was released by GE Healthcare. The transmission component of the scanner was a one-slice CT scanner providing a slice thickness of 10 mm. The transmission x-ray source was mounted on a slip-ring gantry of the Millennium VG gamma camera (GE Healthcare). The x-ray detector system was similar to third-generation CT scanners and was designed to move along with the gamma camera detector system. The time required for one-slice acquisition was about 14 s, and contiguous slices were taken by moving the patient in the axial direction [86].

Coincidence detection was also available since the crystal thickness was thicker than used in regular SPECT systems (16.5 mm). The voltage of the x-ray tube was 140 kVp, and tube current was 2.5 mA, leading to a significant reduction of the x-ray absorbed

dose when compared to standard diagnostic CT machines. With these characteristics, the system was not able to reveal useful diagnostic information but satisfied the requirements of attenuation correction. The CT subsystem could cover the heart in 13–17 slices in a period of 5 min.

The same manufacturer released another SPECT/CT version (GE Infinia Hawkeye-4) that provided a four-slice low-dose CT with fewer demands on room space requirements. The slice thickness of this system was fixed to 5 mm. The system was able to provide adequate attenuation correction and lesion localization with emphasis placed on limited spatial resolution when compared to fully diagnostic CT machines. Furthermore, the volumetric dose index in the acquisition of a head protocol was found to be 8 mGy, in comparison to 42 mGy as measured by DST, which is a 16-slice diagnostic CT used in PET/CT scanners [87]. Other vendors have SPECT/CT systems that are able to provide diagnosticians high-quality and fully diagnostic CT information; thereby, the utility of the CT portion of the hybrid SPECT/CT scanner is no longer concerned with attenuation correction and lesion localization, but its clinical benefits have been extended to other areas of cardiac imaging, such as calculation of calcium scoring and coronary CT angiography. Different SPECT/CT models are shown in Fig. 10.9.

The tube voltage and current are important parameters that determine image quality and levels of the absorbed dose. Vendors vary in their CT specification, such that the tube voltage can be 90–140, 110–130, 120, or 120–140 kVp. Also, the tube current could be as low as 1–2.5 mA or higher, such as 5–80, 20–354, or 20–500 mA. The number of slices has also been increased to 6, 16, 64, or even more, as can be found in the Philips BrightView XCT using a flat-panel CT in which the number of slices is 140 and slice thickness is 1 mm. However, the slice thickness can be lower than 1 mm, in some SPECT/CT scanners reaching a value of 0.6 mm. An important feature of the currently available commercial designs is the high-speed acquisitions using spiral CT generation by which the rotation time can be even less than 0.5 s. This allows for scanning the heart region in one full rotation, minimizing problems of temporal coverage associated with older CT models. Also, it can help reduce the likelihood of patient motion and enhance patient throughput.

One of the disadvantages provided by fully diagnostic CT acquisition is the increased absorbed dose to the subject under examination. As discussed by Kauffman and Di Carli [88], cardiac imaging using hybrid functional and anatomical SPECT/CT is challenged by the high radiation dose to the patients. However, recent approaches to minimize high levels of absorbed doses have been implemented, such as low-dose CT angiography and a reduced amount of injected activity into the patient.

10.5.3 Temporal Mismatch

Another problem also of concern is the differences that arise from temporal data sampling. The CT scan is

Fig. 10.9 (**a**) The Siemens Symbia single-photon emission computed tomography/computed tomography (SPECT/CT) scanner. (**b**) Millennium VG Hawkeye SPECT/CT scanner. (**c**) BrightView XCT, which integrates the SPECT system with flat detector x-ray CT

acquired in a relatively short duration compared to emission acquisition. This actually is a problem especially in the thoracic region as the lung and heart are moving organs and not fixed in one spatial position. The emission images are a temporal average of the organ motion over the respiratory or cardiac cycles. This phenomenon has its undesired consequences in corrupting the attenuation correction and leading to misregistration errors and false interpretation results.

One of the potential applications of SPECT/CT systems is their utility in cardiac imaging, for which better attenuation correction can be performed. However, due to the mentioned limitation, there are recommendations to check the acquired emission/transmission data for possible artifacts [89]. This issue of data misalignment between CT and radionuclide emission scanning has also been found in cardiac PET studies as well as in lung FDG examinations.

Kennedy et al. [90] have recently shown that 23% of the patient studied using cardiac SPECT/CT had a misregistration errors of significant effects and 16% were in the direction of the most severe artifacts [91]. A comparable percentage was also found in Rb-82 cardiac PET/CT scanning with magnitudes of 24.6% and 29.0% in adenosine stress and rest studies, respectively [92]. Misregistration errors resulted in false-positive results in 40% of patients undergoing dipyridamole stress and rest Rb-82 cardiac PET/CT [93]. Another study demonstrated 42% errors in cardiac SPECT/CT images, concluding that careful inspection of attenuation correction maps and registration are needed to avoid reconstruction artifacts due to misregistration [94]. Nonetheless, manual intervention as well as quality control software programs are possible ways to realign the images and improve the correction and imaging task [95].

10.5.4 Other Artifacts

One of the potential applications of SPECT/CT systems is their use in skeletal scintigraphy. Gnanasegaran et al. [96] discussed the most common artifacts associated with bone SPECT/CT. These are SPECT/CT misregistration, respiratory artifacts due to lung motion, arms up or down, metal or contrast agent artifacts, patient size and noise, together with limitations arising from CT scanners. Factors that affect SPECT image quality could be potentially a candidate to cause undesired errors in the coregistered images. The center of rotation and alignment of the two imaging modalities is a pertinent factor in the accuracy and reliability of attenuation correction and image alignment. The existence of a patient's arms in the field of view could also introduce attenuation or truncation artifacts. Metals and high-density materials have the capability of altering the attenuation coefficients and serve to enhance beam hardening effects.

10.5.5 SPECT/CT Applications

The utility of SPECT/CT systems is expanding in many areas of research and clinical practice. In addition to attenuation correction, other image degrading factors can also be accounted for from the use of the CT images. A model-based approach to derive Compton probabilities or transmission-based scatter correction can be applied using CT images to correct for scattered photons, as shown by Willowson et al. [94]. In the same report, the effect of partial volume also was accounted for using the CT data, and all corrections revealed an accurate tracer estimate of 1% with a precision of $\pm 7\%$. In brain studies, correction for partial volume is critical, and reliable and quantitative outcome cannot be obtained without considerations placed on the phenomenon. The binding potential of the striatum can be underestimated by 50% in the absence of partial volume correction. However, in the presence of anatomically guided partial volume correction, substantial improvement can be obtained [97, 98]. In a porcine model, Da Silva et al. [73] showed that an attenuation correction alone for myocardial perfusion Tc-99m-labeled sestamibi cannot yield higher quantitative accuracy without proper correction for partial volume. The combined corrections, however, resulted in higher absolute activity concentrations within a range of 10%. CT data provided an accurate template for modeling the subject anatomy and for accurate definition of the myocardial boundaries (further discussion can be found in Chap. 15).

SPECT/CT systems are also helpful in absorbed dose estimation since the CT images are able to provide a highly accurate assessment of tumor volume. This is an important step in dose calculation schemes required in radioimmunotherapy and other dose

estimation disciplines. As SPECT data can provide important functional information about drug distribution, residence time, and patient follow-up, the additive value of CT can enhance the quantitative accuracy of the measurements for subsequent accurate dose estimates. In the case of pure beta emitters and attempts to image radiotracer distribution based on bremsstrahlung radiation, x-ray CT provides a good anatomical template to delineate and distinguish various tissue uptakes [99].

10.6 Conclusions

The gamma camera is a device with multicompartments. Each of these elements plays a role in the photon detection task and determination of tracer biodistribution. Digital technology and multihead systems were key factors that enhanced and motivated the performance of the gamma camera. Implementations of new camera design with different geometry, fast acquisition protocols, and reconstruction algorithms provide relatively new features for the current and future generations of the gamma camera. Semiconductor systems with room temperature materials and good performance characteristics are of interest among some manufacturers and medical users. Use of new photodetectors would help to enhance the diagnostic quality of nuclear medicine images. They also provide compactness, portability, and better imaging features. The addition of CT as a structural imaging modality to SPECT systems has found numerous applications in many areas of clinical practice as well as in the research setting.

References

1. Patton DD (2003) The birth of nuclear medicine instrumentation: Blumgart and Yens, 1925. J Nucl Med 44(8):1362–1365
2. Graham LS, Kereiakes JG, Harris C, Cohen MB (1989) Nuclear medicine from Becquerel to the present. Radiographics 9(6):1189–1202
3. Anger H (1985) Scintillation camera. Rev Sci Instrum 29:27–33
4. Chandra R (1998) Nuclear medicine physics: the basics, 5th edn. Williams &Wilkins, London
5. Vesel J, Petrillo M (2005) Improved gamma camera performance using event positioning method based on dis-tance dependent weighting. IEEE Nucl Sci Symp Conf Rec 5:2445–2448
6. Kulberg GH, Muehllehner G, van Dijk N (1972) Improved resolution of the Anger scintillation camera through the use of threshold preamplifiers. J Nucl Med 13(2):169–171
7. Ricard M (2004) Imaging of gamma emitters using scintillation cameras. Nucl Instrum Meth Phys Res A 527(1–2):124–129, In: Proceedings of the 2nd international conference on imaging technologies in biomedical sciences
8. Joung J, Miyaoka RS, Kohlmyer S, Lewellen TK (2000) Implementation of ML based positioning algorithms for scintillation cameras. IEEE Trans Nucl Sci 47(3):1104–1111
9. Cherry SR, Sorenson JA, Phelps ME (2003) Physics in nuclear medicine. Saunders, Philadelphia
10. Moore SC, Kouris K, Cullum I (1992) Collimator design for single photon emission tomography. Eur J Nucl Med 19(2):138–150
11. Lau YH, Hutton BF, Beekman FJ (2001) Choice of collimator for cardiac SPET when resolution compensation is included in iterative reconstruction. Eur J Nucl Med 28(1):39–47
12. Murphy PH (1987) Acceptance testing and quality control of gamma cameras, including SPECT. J Nucl Med 28(7):1221–1227
13. Inoue Y, Shirouzu I, Machida T, Yoshizawa Y, Akita F, Doi I, Watadani T, Noda M, Yoshikawa K, Ohtomo K (2003) Physical characteristics of low and medium energy collimators for 123I imaging and simultaneous dual-isotope imaging. Nucl Med Commun 24(11):1195–1202
14. Accorsi R (2008) Brain single-photon emission CT physics principles. Am J Neuroradiol 29(7):1247–1256
15. Peremans K, Cornelissen B, Van Den Bossche B, Audenaert K, Van de Wiele C (2005) A review of small animal imaging planar and pinhole SPECT gamma camera imaging. Vet Radiol Ultrasound 46(2):162–170
16. Wong TZ, Turkington TG, Polascik TJ, Coleman RE (2005) ProstaScint (capromab pendetide) imaging using hybrid gamma camera-CT technology. AJR Am J Roentgenol 184:676–680
17. Kupinski MA, Barrett HH (2005) Small-animal SPECT imaging. Spinger Science + Business Media, New York
18. Giokaris N, Loudos G, Maintas D, Karabarbounis A, Lembesi M, Spanoudaki V, Stiliaris E, Boukis S et al (2005) Partially slotted crystals for a high-resolution g-camera based on a position sensitive photomultiplier. Nucl Instrum Meth Phys Res A 550:305–312
19. Giokaris N, Loudo G, Maintas D, Karabarbounis A, Lembesi M et al (2006) Comparison of CsI(Tl) and CsI(Na) partially slotted crystals for high-resolution SPECT imaging. Nucl Instrum Meth Phys Res A 569:185–187
20. Knoll GF (2000) Radiation detection and measurements, 3rd edn. Wiley, New York
21. Patt BE, Iwanczyk JS, Rossington TC, Wang NW, Tornai MP, Hoffman EJ (1998) High resolution CsI(Tl)/Si-PIN detector development for breast imaging. IEEE Trans Nucl Sci 45(4):2126–2131
22. Garcia EV, Faber TL (2009) Advances in nuclear cardiology instrumentation: clinical potential of SPECT and PET. Curr Cardiovasc Imag Rep 2(3):230–237

23. Walrand S, Jamar F, de Jong M, Pauwels S (2005) Evaluation of novel whole-body high-resolution rodent SPECT (Linoview) based on direct acquisition of linogram projections. J Nucl Med 46:1872–1880

24. Del Guerra A, Di Domenico G, Scandola M, Zavattini G (1998) YAP-PET: first results of a small animal positron emission tomograph based on YAP:Ce finger crystals. IEEE Trans Nucl Sci 45:3105–3108

25. Pani R, Bennati P, Betti M, Cinti MN, Pellegrini R (2006) Lanthanum scintillation crystals for gamma ray imaging. Nucl Instr Meth A 567:294–297

26. Bennati P, Betti M, Cencelli O, Cinti MN, Cusanno F, DeNotaristefani F, Garibaldi F, Karimian A, Mattiolo M et al (2004) Imaging performances of LaCl3:Ce scintillation crystals in SPECT. IEEE Nucl Sci Symp Conf Rec 4: 2283–2287

27. Pani R, Pellegrini R, Cinti MN, Bennati P, Betti M, Vittorini F (2007) LaBr3(Ce) crystal: the latest advance for scintillation cameras. Nucl Instrum Meth A 572 (1):268–269

28. Groch MW, Erwin WD (2001) Single-photon emission computed tomography in the year instrumentation and quality control. J Nucl Med Technol 29:12–18

29. Madsen M (2007) Recent advances in SPECT imaging. J Nucl Med 48(4):661–673

30. Sayeram S, Tsui BMW, De Zhao X, Frey EC (2003) Performance evaluation of three different SPECT systems used in In-111 ProstaScint® SPECT imaging. IEEE Nucl Sci Symp Conf Rec 5:3129–3133

31. Harbert JC, Eckelman WC, Neumann RD (1996) Nuclear medicine: diagnosis and therapy. Thieme Medical, New York

32. http://sales.hamamatsu.com/assets/pdf/catsandguides/PMT_handbook_v3aE.pdf. Accessed 20 Jan 2010

33. Boyd C, Dalrymple G (1974) Basic science principles of nuclear medicine. Mosby, London

34. Buvat I, De Sousa MC, Di Paola M, Ricard M, Lumbroso J, Aubert B (1988) Impact of scatter correction in planar scintimammography: a phantom study. J Nucl Med 39 (9):1590–1596

35. Graham LS, LaFontaine RL, Stein MA (1986) Effects of asymmetric photopeak windows on flood field uniformity and spatial resolution of scintillation cameras. J Nucl Med 27:706–713

36. Collier BD, Palmer DW, Knobel J, Isitman AT, Hellman RS, Zielonka JS (1984) Gamma camera energy windows for Tc-99m bone scintigraphy: effect of asymmetry on contrast resolution. Radiology 151(2):495–497

37. Pani R (2004) Recent advances and future perspectives of position sensitive PMT. Nucl Instrum Meth Phys Res B 213:197–205

38. Kume H, Suzuki S, Takeuchi J, Oba K (1985) Newly developed photomultiplier tubes with position sensitivity capability. IEEE Trans Nucl Sci NS-32(1):448

39. Pichler BJ, Ziegler SI (2004) Photodetectors. In: Wernick M, Aarsvold J (eds) Emission tomography: the fundamentals of PET and SPECT. Elsevier Academic Press, San Diego

40. Del Guerra A, Belcari N, Bisogni MG, Llosá G, Marcatili S, Moehrs S (2009) Advances in position-sensitive photodetectors for PET applications. Nucl Instrum Meth Phys Res A 604(1–2):319–322

41. Dornebos P, van Eijk CW (1995) In: Proceedings of the international conference on inorganic scintillators and their applications. Delft University of Technology, Delft, The Netherlands, 28 August–1 September 1995

42. Loudos GK, Nikita KS, Uzunoglu NK, Giokaris ND, Papanicolas CN, Archimandritis SC et al (2003) In: SCINT95, Proceedings of the international conference on inorganic scintillators and their applications. Improving spatial resolution in SPECT with the combination of PSPMT based detector and iterative reconstruction algorithms. Comput Med Imaging Graph 27(4):307–313

43. Del Guerra A, Di Domenico G, Scandola M, Zavattini G (1998) High spatial resolution small animal YAPPET. Nucl Instrum Meth Phys Res A 409:537–541

44. Pani R, Pellegrini R, Cinti MN, Trotta C, Trotta G, Scafe R, Betti M et al (2003) A novel compact gamma camera based on flat panel PMT. Nucl Instrum Meth Phys Res A 513:36–41

45. Renker D (2007) New trends on photodetectors. Nucl Instrum Meth Phys Res A 571:1–6

46. Lecomte R (2009) Novel detector technology for clinical PET. Eur J Nucl Med Mol Imaging 36(Suppl 1):S69–S85

47. Lewellen TK (2008) Recent developments in PET detector technology. Phys Med Biol 53(17):R287–R317

48. Pichler B, Lorenz E, Mirzoyan R, Pimpl W, Roder F, Schwaiger M, Ziegler SI (1997) Performance test of a LSO-APD PET module in a 9.4 tesla magnet. IEEE Nucl Sci Symp 2:1237–1239

49. Shah KS, Farrell R, Grazioso R, Harmon ES, Karplus E (2002) Position-sensitive avalanche photodiodes for gamma-ray imaging. Nucl Sci IEEE Trans Nucl Sci 49 (4):1687–1692

50. Yang Y, Wu Y, Qi J, St. James S, Huini Du A, Dokhale P, Shah K et al (2008) A prototype PET scanner with DOI-encoding detectors. J Nucl Med 49:1132–1140

51. Burr KC, Ivam A, Castleberry DE, LeBlanc JW, Shah KS, Farrell R (2004) Evaluation of a prototype small-animal PET detector with depth-of-interaction encoding. IEEE Trans Nucl Sci 51:1791–1798

52. Yang Y, Dokhale PA, Silverman RW, Shah KS, McClish MA, Farrell R, Entine G, Cherry SR (2006) Depth of interaction resolution measurements for a high resolution PET detector using position sensitive avalanche photodiodes. Phys Med Biol 51:2131–2142

53. Funk T, Després P, Barber WC, Shah KS, Hasegawa BH (2006) Multipinhole small animal SPECT system with submillimeter spatial resolution. Med Phys 33(5):1259–1268

54. Renker D (2006) Geiger-mode avalanche photodiodes, history, properties and problems. Nucl Instrum Meth Phys Res A 567:48–56

55. Otte N, Dolgoshein B, Hose J, Klemin S, Lorenz E, Mirzoyan R et al (2006) The SiPM – a new photon detector for PET, nuclear physics B. In: Proceedings of the 9th topical seminar on innovative particle and radiation detectors, vol 150, pp 417–420

56. Schaart DR, van Dam HT, Seifert S, Vinke R, Dendooven P, Löhner H, Beekman FJ (2009) A novel, SiPM-array-

based, monolithic scintillator detector for PET. Phys Med Biol 54:3501

57. Maas MC, Schaart DR, van der Laan DJ, Bruyndonckx P, Lemaître C, Beekman FJ, van Eijk CW (2009) Monolithic scintillator PET detectors with intrinsic depth-of-interaction correction. Phys Med Biol 54(7):1893–1908

58. Wagennar DJ (2004) CdTe and CdZnTe semiconductor detectors for nuclear medicine imaging. In: Wernick MN, Aarsvold JN (eds) Emission tomography. The fundamentals of PET and SPECT. Elsevier, San Diego

59. Mori I, Takayama T, Motomura N (2001) The CdTe detector module and its imaging performance. Ann Nucl Med 15(6):487–494

60. Gambhir SS, Berman DS, Ziffer J, Nagler M, Sandler M, Patton J, Hutton B, Sharir T, Haim SB, Haim SB (2009) A novel high-sensitivity rapid-acquisition single-photon cardiac imaging camera. J Nucl Med 50(4):635–643

61. Berman DS, Kang X, Tamarappoo B, Wolak A, Hayes SW, Nakazato R, Thomson LE, Kite F, Cohen I, Slomka PJ, Einstein AJ, Friedman JD (2009) Stress thallium-201/rest technetium-99m sequential dual isotope high-speed myocardial perfusion imaging. JACC Cardiovasc Imaging 2(3):273–282

62. Erlandsson K, Kacperski K, van Gramberg D, Hutton BF (2009) Performance evaluation of D-SPECT: a novel SPECT system for nuclear cardiology. Phys Med Biol 54:2635–2649

63. Keidar Z, Kagna O, Frenkel A, Israel O (2009) A novel ultrafast cardiac scanner for myocardial perfusion imaging (MPI): comparison with a standard dual-head camera. J Nucl Med 50(Suppl 2):478

64. Taillefer R (2005) Clinical applications of 99mTc-sestamibi scintimammography. Semin Nucl Med 35:100–115

65. Mueller B, O'Connor MK, Blevis I, Rhodes DJ, Smith R, Collins DA, Phillips SW (2003) Evaluation of a small cadmium zinc telluride detector for scintimammography. J Nucl Med 44(4):602–609

66. Pani R, Pellegrini R, Cinti MN, Bennati P, Betti M, Casali V et al (2006) Recent advances and future perspectives of gamma imagers for scintimammography. Nucl Instrum Meth A 569:296–300

67. Blevis Ira M, O'Conner MK, Keidar Z, Pansky A et al (2006) CZT for scintimammography. Phys Med 21(Suppl 1):56–59

68. Stout DB, Zaidi H (2008) Preclinical multimodality imaging in vivo. PET Clin 3(3):251–273

69. Keidar Z, Israel O, Krausz Y (2003) SPECT/CT in tumor imaging: technical aspects and clinical applications. Semin Nucl Med 33(3):205–218

70. Garcia EV (2007) SPECT attenuation correction: an essential tool to realize nuclear cardiology's manifest destiny. J Nucl Cardiol 14:16–24

71. Germano G, Slomka PJ, Berman DS (2007) Attenuation correction in cardiac SPECT: the boy who cried wolf? J Nucl Cardiol 14:25–35

72. Da Silva AJ, Tang HR, Wong KH, Wu MC, Dae MW, Hasegawa BH (2001) Absolute quantification of regional myocardial uptake of 99mTc-sestamibi with SPECT: experimental validation in a porcine model. J Nucl Med 42(5):772–779

73. Ellis RJ, Kim EY, Conant R et al (2001) Radioimmuno-guided imaging of prostate cancer foci with histopathological correlation. Int J Radiat Oncol Biol Phys 49:1281–1286

74. Ritman EL (2007) Small-animal CT – its difference from, and impact on, clinical CT. Nucl Instrum Meth Phys Res A 580(2):968–970

75. Kuhl DE, Hale J, Eaton WL (1966) Transmission scanning: a useful adjunct to conventional emission scanning for accurately keying isotope deposition to radiographic anatomy. Radiology 87(2):278–284

76. Patton JA, Townsend DW, Hutton BF (2009) Hybrid imaging technology: from dreams and vision to clinical devices. Semin Nucl Med 39(4):247–263

77. Bailey DL, Hutton BF, Walker PJ (1987) Improved SPECT using emission and transmission tomography. J Nucl Med 28:844–851

78. Tsui BM, Gullberg GT, Edgerton ER et al (1989) Correction of nonuniform attenuation in cardiac SPECT imaging. J Nucl Med 30:497–507

79. Slomka PJ, Baum RP (2009) Multimodality image registration with software: state-of-the-art. Eur J Nucl Med Mol Imaging 36(Suppl 1):S44–S55

80. West J, Fitzpatrick JM, Wang MY, Dawant BM, Maurer CR, Kessler RM et al (1997) Comparison and evaluation of retrospective intermodality brain image registration techniques. J Comput Assist Tomogr 21(4):554–566

81. Beyer T, Pichler B (2009) A decade of combined imaging: from a PET attached to a CT to a PET inside an MR. Eur J Nucl Med Mol Imaging 36:S1–S144

82. Seibert JA, Boone JM (2005) X-ray imaging physics for nuclear medicine technologists. Part 2: X-ray interactions and image formation. J Nucl Med Technol 33(1):3–18

83. Darambara DG (2006) State-of-the-art radiation detectors for medical imaging: demands and trends. Nucl Instrum Meth Phys Res A 569(2):153–158

84. Saoudi A, Lecomte R (1999) A novel APD-based detector module for multi-modality PET/SPECT/CT scanners. IEEE Trans Nucl Sci 46(3):479–484

85. Cherry SR (2009) Multimodality imaging: beyond PET/CT and SPECT/CT. Semin Nucl Med 39(5):348–353

86. Bocher M, Balan A, Krausz Y, Shrem Y, Lonn A, Wilk M, Chisin R (2000) Gamma camera-mounted anatomical X-ray tomography: technology, system characteristics and first images. Eur J Nucl Med 27(6):619–627

87. Hamann M, Aldridge M, Dickson J, Endozo R, Lozhkin K, Hutton BF (2008) Evaluation of a low-dose/slow-rotating SPECT-CT system. Phys Med Biol 53:2495–2508

88. Kaufmann PA, Di Carli MF (2009) Hybrid SPECT/CT and PET/CT imaging: the next step in noninvasive cardiac imaging. Semin Nucl Med 39(5):341–347

89. Goetze S, Wahl RL (2007) Prevalence of misregistration between SPECT and CT for attenuation-corrected myocardial perfusion SPECT. J Nucl Cardiol 14(2):200–206

90. Kennedy JA, Israel O, Frenkel A (2009) Directions and magnitudes of misregistration of CT attenuation-corrected myocardial perfusion studies: incidence, impact on image quality, and guidance for reregistration. Nucl Med 50(9):1471–1478

91. Kennedy JA, Israel O, Frenkel A (2009) Directions and magnitudes of misregistration of CT attenuation-corrected

myocardial perfusion studies: incidence, impact on image quality, and guidance for reregistration. J Nucl Med 50 (9):1471–1478

92. Schuster DM, Halkar RK, Esteves FP, Garcia EV, Cooke CD, Syed MA, Bowman FD, Votaw JR (2008) Investigation of emission-transmission misalignment artifacts on rubidium-82 cardiac PET with adenosine pharmacologic stress. Mol Imaging Biol 10(4):201–208

93. Gould KL, Pan T, Loghin C, Johnson NP, Guha A, Sdringola S (2007) Frequent diagnostic errors in cardiac PET/CT due to misregistration of CT attenuation and emission PET images: a definitive analysis of causes, consequences, and corrections. J Nucl Med 48:1112–1121

94. Willowson K, Bailey DL, Baldock C (2008) Quantitative SPECT reconstruction using CT-derived corrections. Phys Med Biol 53(12):3099–3112

95. Chen J, Caputlu-Wilson SF, Shi H, Galt JR, Faber TL, Garcia EV (2006) Automated quality control of emission-transmission misalignment for attenuation correction in myocardial perfusion imaging with SPECT-CT systems. J Nucl Cardiol 13(1):43–49

96. Gnanasegaran G, Barwick T, Adamson K, Mohan H, Sharp D, Fogelman I (2009) SPECT/CT in benign and malignant bone disease: when the ordinary turns into the extraordinary. Semin Nucl Med 39(6):431–442

97. Soret M, Koulibaly PM, Darcourt J, Hapdey S, Buvat I (2003) Quantitative accuracy of dopaminergic neurotransmission imaging with 123I SPECT. J Nucl Med 44(7):1184–1193

98. Vanzi E, De Cristofaro MT, Ramat S, Sotgia B, Mascalchi M, Formiconi AR (2007) A direct ROI quantification method for inherent PVE correction: accuracy assessment in striatal SPECT measurements. Eur J Nucl Med Mol Imaging 34(9):1480–1489

99. D'Asseler Y (2009) Advances in SPECT imaging with respect to radionuclide therapy. Q J Nucl Med Mol Imaging 53:343–347

100. Riboldi S, Seidel J, Green M, Monaldo J, Kakareka J, Pohida T (2003) Investigation of signal readout methods for the Hamamatsu R8500 flat panel PSPMT. *Nuclear Science Symposium Conference Record, 2003 IEEE* 4:2452–2456

101. Xie Q, Chien-Min Kao, Byrum K, Drake G, Vaniachine A, Wagner RG, Rykalin V, Chin-Tu Chen (2006) Characterization of Silicon Photomultipliers for PET Imaging. *Nuclear Science Symposium Conference Record, 2006. IEEE* 2:1199–1203